CONF-9008125--9

SAND--90-0897C

DE91 004569

PLANAR-SHOCK AND PENETRATION RESPONSE OF CERAMICS

M. E. KIPP, D. E. GRADY, and J. L. WISE

Sandia National Laboratories
Albuquerque, New Mexico 87185, U. S. A.

Two high-strength ceramic materials (boron carbide and titanium diboride) have been subjected to both planar shock and long-rod penetration, and their response has been characterized with time-resolved particle-velocity measurements. In symmetric planar impacts at 1500 and 2200 m/s, shock stresses ranged between 20 and 50 GPa. To examine the ceramic response to divergent waves, targets containing a ceramic layer were impacted at a nominal velocity of 1600 m/s by a 2-mm diameter tungsten penetrator at normal incidence. Penetration targets were built with, and without, a steel cover plate to examine the influence of confinement. Preliminary wavecode analyses of the ceramic response are included.

I. INTRODUCTION

Ceramics have been repeatedly demonstrated to be effective armor materials against a variety of threats (*e.g.*, Wilkins, *et al.* [1]). Planar impact data for the two ceramics discussed here, boron carbide (B_4C) and titanium diboride (TiB_2), may be found in the collection of Hugoniot data that has been assembled by Gust and Royce [2] and Gust, *et al.* [3], including Hugoniot elastic limits (HEL) and shock Hugoniots for about a dozen ceramic materials. Some shock wave data are also available for titanium diboride [4].

Wave profile data in compression and release in uniaxial strain are presented here for B_4C and TiB_2 (See Ref.[5] for additional details).

In addition to the planar impact experiments, targets containing a ceramic layer were impacted by a long-rod penetrator at normal incidence [6]. The longitudinal particle-velocity history on the rear free surface of the target was monitored on the penetration axis. The diverging waves in the target plate create a velocity record that depends on the impact and penetration process, even though the recording point is spatially removed from the impact point. The one-dimensional (uniaxial strain) data are invaluable in the construction of material models; the divergent data can be directly compared with primary code variables (*e.g.,* particle velocity) to evaluate multidimensional calculations, complementing flash x-ray data (which supply global "snapshots" of the flow field at a few discrete times) and penetration performance (*i.e.,* ballistic limit) data.

II. PLATE IMPACT EXPERIMENTS

Uniaxial strain compressive shock and release waves were produced in the ceramics of interest with a single-stage powder gun (89-mm bore diameter, 2200 m/s maximum impact velocity). The ceramic carried by the projectile was backed by foam, and the target consisted of a disc of similar ceramic backed by an optical-quality single crystal of lithium fluoride. The history of the compression and release wave formed by this impact configuration is measured by monitoring the time-resolved longitudinal motion of the ceramic/lithium fluoride interface using laser velocity interferometry (VISAR) techniques [7] (resolution $\sim$ 1 ns). The impact velocity and experimental dimensions for each test are provided in Table 1, and the acquired time-resolved velocity profiles are displayed in Figure 1. (The arrival times of the wave profiles were offset to display the records.)

Table 1: Conditions for Ceramic Plate-Impact Experiments

Material	Impact Velocity (m/s)	Foam Density (kg/m^3)	Impactor Thickness (mm)	Target Thickness (mm)
B_4C	1546	320	3.920	9.044
B_4C	2210	640	3.917	9.033
TiB_2	1515	320	3.972	10.804
TiB_2	2113	640	3.337	10.747

A. MATERIALS

Ultrasonic longitudinal, C_L, and shear, C_S, wave speeds, and reference density, ρ_O, were determined for the ceramic specimens. A summary of these experimental values, accompanied by calculated values for bulk wave speed, C_O, and Poisson's ratio, ν, is provided in Table 2. The titanium diboride was determined to be about 1% porous. Optical microscopy revealed fine-grained, equiaxial grain structures for all samples, with nominal grain sizes of 10 μm for B_4C, and 12 μm for TiB_2.

Table 2: Elastic Properties

Material	ρ_O kg/m^3	C_L m/s	C_S m/s	C_O m/s	ν
B_4C	2516	14040	8900	9570	0.164
TiB_2	4452	10930	7300	6960	0.097

B. COMPRESSION AND RELEASE PROPERTIES

The wave profiles shown in Figure 1 are distorted somewhat in both amplitude and shape due to the mechanical impedance difference between the lithium fluoride and ceramic. Insight into the ceramic response to shock loading is gained by transforming the particle-velocity history for each experiment into a stress-strain load/release curve. In this way, features in the measured wave profiles associated with wave interactions caused by the sample and window material impedance mismatch can be separated from material response properties of the ceramics (yield, phase transformations, *etc.*). Using the one-dimensional explicit Lagrangian shock-wave propagation code, WONDY [8], neither of these ceramics could be readily represented with traditional elastic/perfectly-plastic material models, (primarily a consequence of the inability to accommodate the very dispersive nature of the unloading wave). To obtain accurate internal stress/strain histories, a parametrized load/unload path was incorporated into WONDY, and exercised in an iterative fashion [9], until the VISAR interface particle-velocity history for each experiment was reproduced. (We have assumed that the primary contribution to the stress is the material strain, and any dependence on both strain rate and thermal effects has been neglected.) Ultrasonic data were used to define the initial loading moduli. Load/release paths at the center of the ceramic target are displayed in Figure 2. Note that, although there is almost a factor of two difference in densities, the elastic loading curves of B_4C and TiB_2 are very nearly identical in both low- and high-amplitude cases. The B_4C shows a major loss in strength when compared to TiB_2.

The Hugoniot elastic limits for these ceramics were determined directly from the measured particle-velocity profiles, $u_M(t)$ (Figure 1), accounting for the impedance mismatch between ceramic and window [5]. The Hugoniot elastic limit data (σ_{HEL}) and the corresponding Hugoniot shock pressure, P_H, are tabulated in Table 3. For the titanium diboride, a reasonably well-defined break in both waves at approximately 160 m/s was tentatively selected as a preliminary yield process or phase transformation u_M value. A second break identified at about 420 m/s is a consequence of some structuring feature in the TiB_2 material response.

Table 3: Hugoniot Elastic Limits

Test No.	Material	u_M (m/s)	σ_{HEL} (GPa)	P_H (GPa)
1	B_4C	580±30	14.8	22.8
2	B_4C	550±40	14.0	31.4
3	TiB_2	165±15	5.2	31.0
"	"	430±40	13.7*	"
4	TiB_2	150±15	4.7	48.5
"	"	410±20	13.1*	"

* Corresponds to second yield structure in TiB_2

III. ROD IMPACT EXPERIMENTS

The penetration experiments [6] employed a 2-mm diameter, 20-mm long tungsten-alloy rod which impacted a nominally 5-mm or 10-mm thick, 76-mm diameter target plate of ceramic that was backed, in turn, by a 2-mm thick, 51-mm diameter buffer disk of OFHC copper. In some cases, a 2-mm steel cover plate was included to increase confinement. Normal incidence of the penetrator was maintained by mounting it rigidly in the projectile nosepiece. The projectile assembly was accelerated by a single-stage powder gun (89-mm bore diameter) to a nominal impact velocity of 1600 m/s. The particle-velocity history at an observation point, located on the penetration axis on the back surface of the copper buffer, was measured with a velocity interferometer (VISAR [7]).

A. MATERIALS

The target-plate materials were boron carbide and titanium diboride. Ultrasonic longitudinal, C_L, and shear, C_S, wave speeds, and reference density, ρ_O, were determined for the penetrator and the target components in this study. A summary of these properties, accompanied by calculated values for bulk wave speed, C_O, and Poisson's ratio, ν, is provided in Table 4. Minor differences in ceramic properties are visible compared with the data in Table 2.

Table 4: Elastic Properties

Material	ρ_O kg/m^3	C_L m/s	C_S m/s	C_O m/s	ν
B_4C	2517	14140	8897	9717	0.1723
TiB_2	4509	10850	7450	6610	0.0538
AISI 4340	7810	5884	3202	4578	0.2897
OFHC Cu	8920	4689	2250	3904	0.3506
W-Alloy	17250	5164	2837	3993	0.2840

B. RESULTS

Particle-velocity histories are reported here for one test on a target of B_4C, and four on

targets of TiB_2. For each experiment, Table 5 lists the target material, steel confinement thickness, t_{CON}, target thickness, t_{TAR}, copper buffer thickness, t_{BUF}, tungsten-rod impact velocity, V, and transit time, τ, of the leading toe of the wave disturbance through the target assembly. The duplicate experiments (1,2) for TiB_2 established the reproducibility of the VISAR data, and suggested which fine, "non-average" details of the wave profiles were not attributable to special material properties.

Table 5: Conditions for Rod Impact Experiments

Target Material	t_{CON} (mm)	t_{TAR} (mm)	t_{BUF} (mm)	V (m/s)	τ (μs)
B_4C		9.69	1.94	1541	1.07
TiB_2 (1)		10.19	2.00	1558	1.33
TiB_2 (2)		10.18	2.00	1567	1.36
TiB_2	1.94	10.20	1.94	1562	1.66
TiB_2	1.94	5.14	2.02	1566	1.23

The experimental records for the TiB_2 are shown in Figure 3. In all cases, there is an initial peak in particle velocity followed by a temporary drop. The B_4C record (Figure 4) contains some noise during the decay period following the initial peak similar to that observed in uniaxial strain records for B_4C.

C. CALCULATIONS

The initial calculations corresponding to these penetration experiments were made with standard elastic/perfectly-plastic material models in the Eulerian wave-propagation code CTH [10]. At the stress levels induced by the given impact velocities, the equation of state for each material is governed by the Gruneisen coefficient, Γ, and a linear shock velocity (U_S) *vs.* particle velocity (U_P) relationship, $U_S = C_O + S\ U_P$, where S is the slope and C_O is the bulk sound speed. An initial yield strength, Y_O, is required, and a fracture strength, σ_F, is assumed for the material. These parameters (summarized in Table 6) coupled with the elastic properties in Table 4 are sufficient to make a first estimate of material response. In the code, mixed-cell yield was set to zero.

Table 6: Computational Parameters

Material	S	Γ	Y_O (GPa)	σ_F (GPa)
B_4C	1.0	1.0	12.8	0.4
TiB_2	1.0	1.0	15.9	0.3
OFHC Cu	1.489	1.99	0.7	0.3
W-Alloy	1.237	1.54	1.3	1.4

The calculated free-surface particle velocities for the unconfined cases are plotted in Figures 4 and 5. As expected from the uniaxial-strain data [5], the calculations for the

ceramic targets clearly lack specific agreement with the experimental data, although the general trends are captured. One aspect of ceramic material response not contained by the elastic/perfectly-plastic model is compressive failure.

IV. CONCLUSIONS

The high-resolution data in the present uniaxial and divergent geometries provide ample opportunity to evaluate code and material model behavior in a quantitative manner. The boron carbide and titanium diboride disperse the release waves more widely than should be the case for normal solid response, suggesting that internal damage during compression has altered the state of the material. It is clear that simple material models generally follow the behavioral trends, but do not capture the detailed response of these ceramic materials, suggesting that more advanced material models are required.

ACKNOWLEDGEMENTS

The authors are indebted to D. E. Cox and R. L. Moody for their careful completion of these experiments, and to J. H. Gieske for his thorough ultrasonic characterization of all test materials. This work performed at Sandia National Laboratories supported by the U.S. Department of Energy under contract DE-AC04-76DP00789.

REFERENCES

1. M. L. Wilkins, C. F. Cline, and C. A. Honodel, *Lawrence Radiation Laboratory Report UCRL-71817* (1969).
2. W. H. Gust and E. B. Royce, *J. Appl. Phys. 42:* (1971) 276.
3. W. H. Gust, A. C. Holt, and E. B. Royce, *J. Appl. Phys. 44:* (1973) 550.
4. D. Yaziv and N. S. Brar, *J. de Physique, Colloque C3, 49:* (1988) 683.
5. M. E. Kipp and D. E. Grady, *Sandia National Laboratories Report SAND89-1461* (1989).
6. J. L. Wise and M. E. Kipp, *Shock Compression of Condensed Matter - 1989, Ed. by S. C. Schmidt, J. N. Johnson, L. W. Davison*, North-Holland (1990) 943.
7. L. M. Barker and R. E. Hollenbach, *J. Appl. Phys. 43:* (1972) 4669.
8. M. E. Kipp and R. J. Lawrence, *Sandia National Laboratories Report SAND81-0930* (1982).
9. D. E. Grady and M. D. Furnish, *Sandia National Laboratories Report SAND88-1642* (1988).
10. J. M. McGlaun, F. J. Zeigler, S. L. Thompson, and M. G. Elrick, *Sandia National Laboratories Report SAND88-0523* (1988).

Figure Captions

Fig. 1 *Plate-impact particle velocity data for B_4C and TiB_2.*

Fig. 2 *Summary of calculated stress/strain load and release paths for B_4C and TiB_2 at the center of the ceramic target.*

Fig. 3 *Rod impact particle-velocity data for TiB_2.*

Fig. 4 *Particle-velocity data and calculation for TiB_2.*

Fig. 5 *Particle-velocity data and calculation for B_4C.*

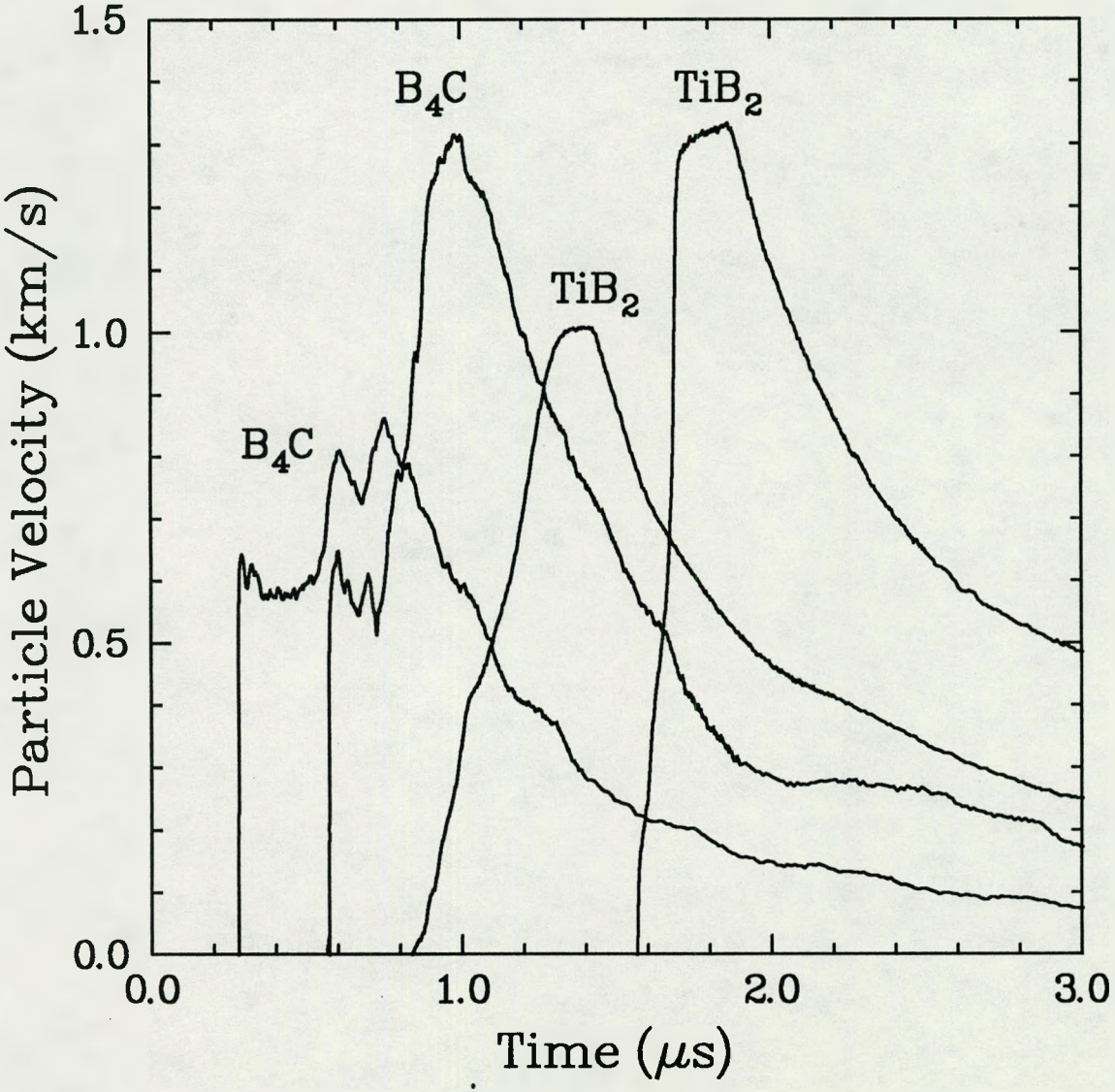
1.5
1.0
0.5
0.0
Particle Velocity (km/s)
B4C
TiB2
TiB2
B4C
0.0
1.0
2.0
3.0
Time (μs)

FIG. 1

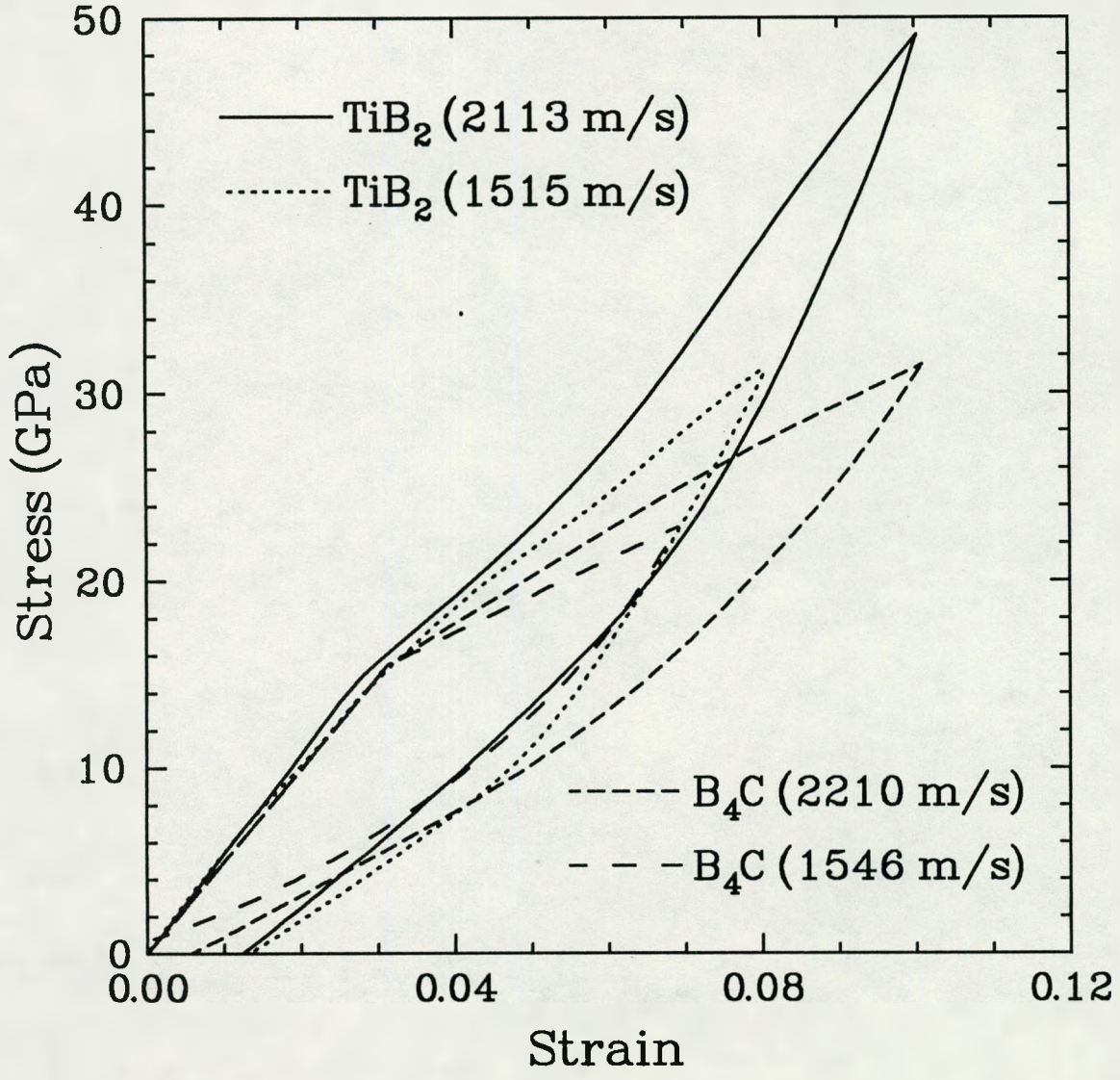
50
40
30
20
10
0
0.00
0.04
0.08
0.12
Stress (GPa)
Strain
TiB2 (2113 m/s)
TiB2 (1515 m/s)
B4C (2210 m/s)
B4C (1546 m/s)

FIG. 2

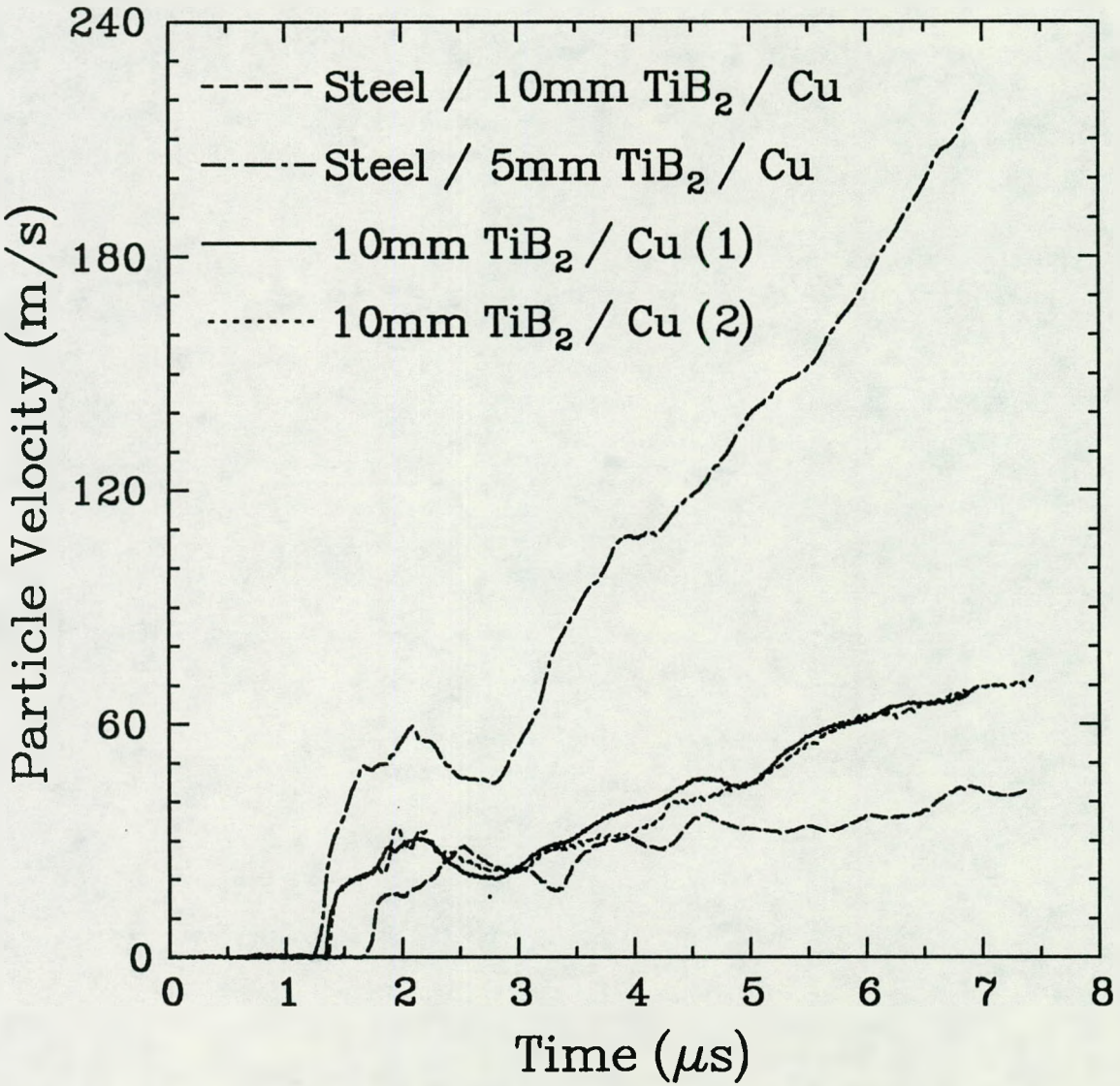
Steel / 10mm TiB2 / Cu
Steel / 5mm TiB2 / Cu
10mm TiB2 / Cu (1)
10mm TiB2 / Cu (2)
Particle Velocity (m/s)
Time (μs)
0
60
120
180
240
0
1
2
3
4
5
6
7
8

FIG. 3

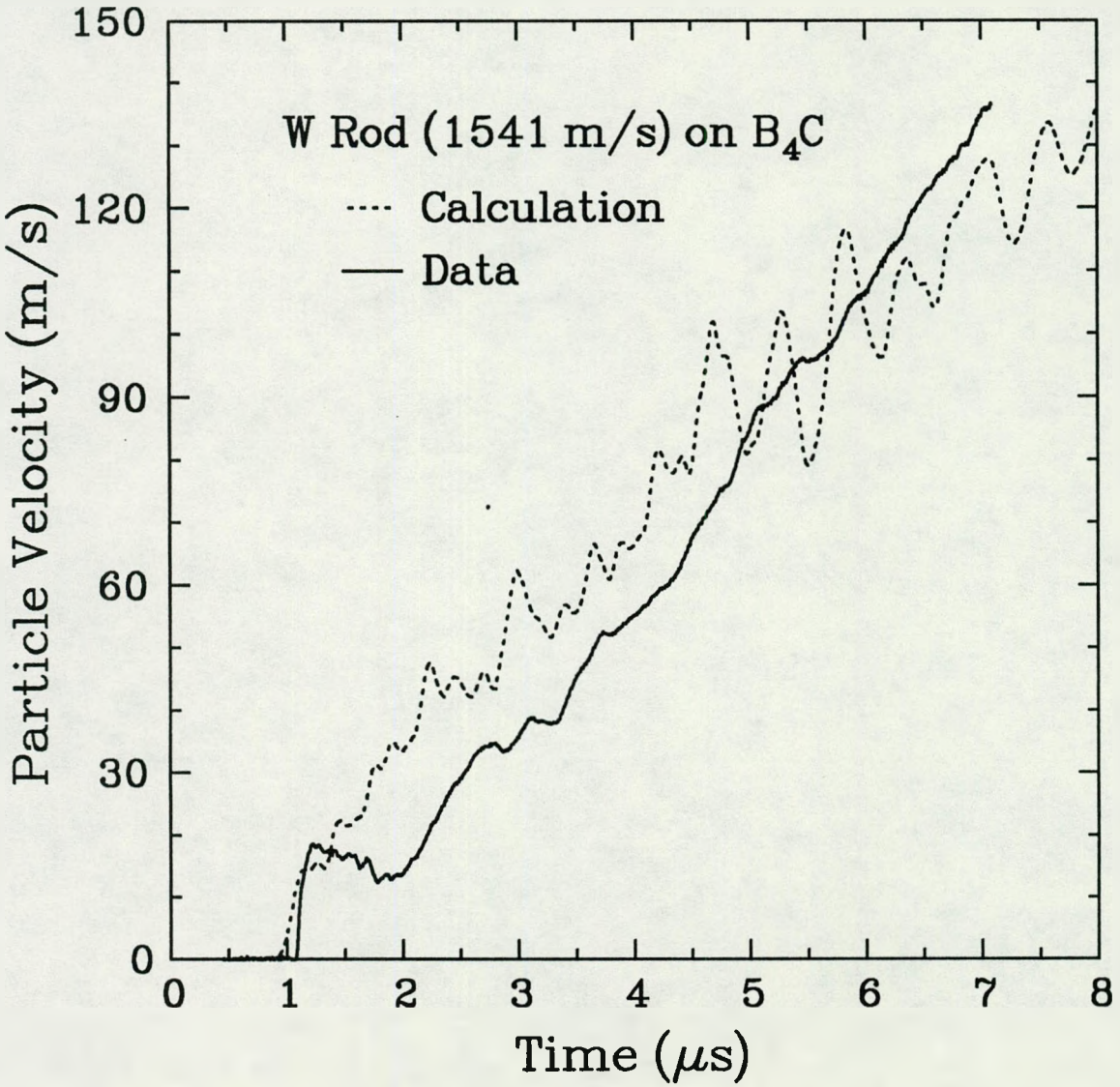
W Rod (1541 m/s) on B_4C
Calculation
Data
Particle Velocity (m/s)
Time (μs)
0
30
60
90
120
150
0
1
2
3
4
5
6
7
8

FIG. 4

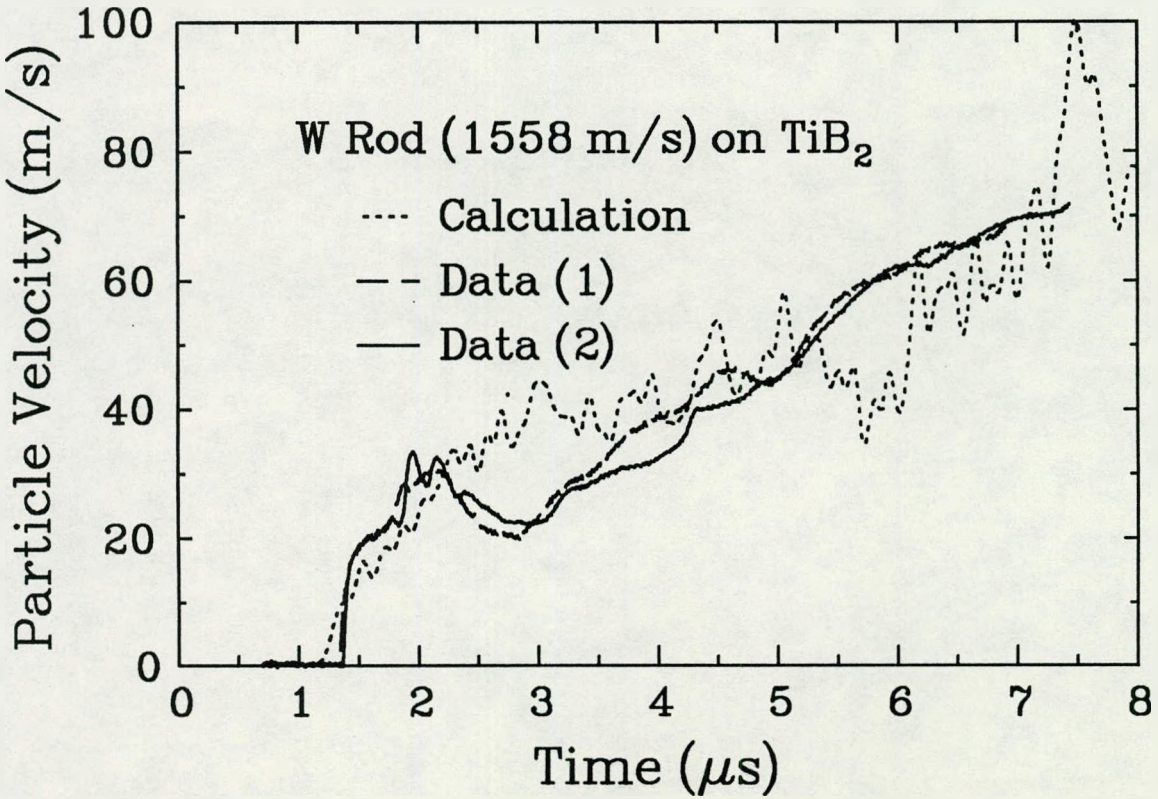
W Rod (1558 m/s) on TiB_2
Calculation
Data (1)
Data (2)
Particle Velocity (m/s)
Time (μs)
0
20
40
60
80
100
0
1
2
3
4
5
6
7
8

FIG. 5